Midinfrared Pulse Generation by Pumping in the Normal-Dispersion Regime of a Gas-Filled Hollow-Core Fiber

Md Imran Hasan,[1,*] Nail Akhmediev,[1] Arnaud Mussot,[2] and Wonkeun Chang[3]

[1] *Optical Sciences Group, Research School of Physics and Engineering, The Australian National University, Acton ACT 2601, Australia*

[2] *University of Lille, CNRS, UMR 8523—PhLAM—Physique des Lasers Atomes et Molécules, Lille, France*

[3] *School of Electrical and Electronic Engineering, Nanyang Technological University, Singapore 639798*

(Received 22 January 2019; revised manuscript received 1 June 2019; published 26 July 2019)

We demonstrate, numerically, the generation of supercontinuum using a high-power ultrafast source at 1.06-μm wavelength and a nonlinear hollow-core fiber. We yield a system that is less sensitive to noise by pumping in the normal-dispersion regime, yet still achieves enhanced spectral broadening by exciting an optical soliton in the midinfrared region. The pump pulse goes through a series of nonlinear effects leading to a supercontinuum output that spans across the midinfrared, 0.5–4.2 μm.

DOI: 10.1103/PhysRevApplied.12.014050

I. INTRODUCTION

Supercontinuum (SC) generation is a nonlinear optical process that allows light with a superbroad bandwidth to be obtained. It has a wide range of implications in many areas of science and technology, including telecommunications [1], microscopy [2], metrology [3], and medicine [4]. While techniques for generating SC in the visible and near-infrared regions are well established and such sources have become commercially available [5], progress in the midinfrared (mid-IR) or far-infrared regions is lacking, with many challenges that need to be addressed. The main difficulty lies in both the availability of efficient pump sources as well as suitable nonlinear media. As for the pump source, there are only a handful of ultrafast laser systems to choose from for pumping in the mid-IR [6]. For a nonlinear medium, soft-glass materials, such as fluoride- and chalcogenide-based materials, have been largely successful for generating SC in the mid-IR [7,8], but their low material-damage threshold and poor mechanical strength impose ultimate limits on the achievable output power of SC.

An approach lacking these deficiencies is to use a nonlinear hollow-core fiber [9]. In a hollow-core fiber, light is tightly confined and guided in the central hollow region, allowing the transmission of a high-power beam along the fiber over a much broader spectral region deep into the mid-IR [10]. The nonlinear phase shift and the corresponding spectral broadening can be induced by filling the fiber with a nonlinear medium, such as high-pressure xenon [11,12]. Several recent studies have shown that this alternative approach can generate SC reaching the mid-IR region [12–14].

One of the decisive parameters that determines the propagation dynamics of ultrashort pulses in nonlinear dispersive media and hence the SC output is the sign of the dispersion at the pump wavelength. Most of the SC-generation sources studied so far, as well as the commercial SC sources, utilize pumping in the anomalous-dispersion regime. They take advantage of the rich optical-soliton dynamics to obtain superbroad spectra [15]. The other possibility is to pump in the normal-dispersion regime. This scheme, although not widely adopted yet, is very attractive because of its stable and coherent SC output that is not sensitive to the noise in the system [16].

In this article, we demonstrate, numerically, how the advantages of both dispersion regimes can simultaneously be utilized in SC generation in a nonlinear hollow-core fiber. Namely, we yield a system that is less sensitive to noise or input-pulse fluctuations by pumping in the normal-dispersion regime, yet still achieves exceptional spectral broadening, particularly toward the long-wavelength edge, by exciting an optical soliton in the anomalous-dispersion regime. At the same time, we present an alternative pathway to generate ultrashort mid-IR pulses efficiently by pumping in the near-infrared, i.e., in the one-micron region where many compact, robust, high-power, and high-beam-quality ultrafast-fiber lasers are readily available. The development of high-average-power ultrafast mid-IR sources is currently of great interest due to their various applications, including remote sensing [4], thermal imaging [17], medical surgery [10], and military applications [18]. Most of the existing high-power mid-IR sources are based on parametric frequency

*imran.hasan@anu.edu.au

conversions, which are often very susceptible to the operation environment, requiring constant alignment and maintenance [6]. A compact and robust alternative, such as the fiber-based mid-IR source that we present herein, offers an attractive solution.

II. LIGHT-GUIDING PROPERTIES OF XENON-FILLED HOLLOW-CORE FIBER

Recent investigations have shown that among many different types of hollow-core fibers, negative-curvature fibers exhibit superior light-guiding properties [19]. Therefore, we consider a simple negative-curvature fiber with six cladding tubes, as shown in the inset of Fig. 1. We set the core diameter $D = 80\ \mu$m, the cladding-tube diameter $d = 60\ \mu$m, the glass-web thickness $t_g = 0.35\ \mu$m, and the perimeter gap between two adjacent cladding tubes $g = 10\ \mu$m.

Figure 1 shows the transmission loss of the fiber's fundamental mode, as well as its percentage power fraction in the glass region, which we obtained using the finite-element method. Particular attention should be paid to the mid-IR, as the silica material is highly absorbent in this region. The figure shows that the mode has a transmission loss of less than 8 dB m^{-1} and a light-glass overlap of less than 0.03% over the entire spectral range presented (0.9–4 μm), making it a good candidate for mid-IR guidance over a length scale of a few centimeters.

We obtain the group-velocity dispersion (GVD) and the effective area of the fiber's fundamental mode by applying the empirical formulas presented in Ref. [20]. We can achieve the sufficiently high nonlinearity required for the spectral broadening by filling the fiber with a heavy gas, such as xenon at high pressure [12]. This compensates for the loss of intensity due to having a relatively large mode area, which is necessary for a low-loss guidance in the mid-IR. Figure 2 presents the GVD and the nonlinear parameter

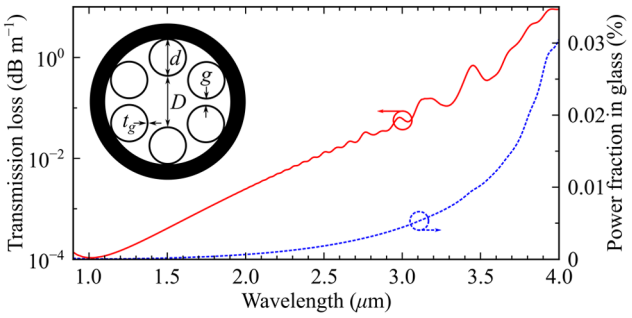

FIG. 1. The transmission loss (red solid line) and percentage power fraction of light in the glass (blue dashed line), calculated for the fundamental mode in the fiber using the finite-element method. The inset shows an idealized cross section of the silica-based negative-curvature fiber. $D = 80\ \mu$m, $d = 60\ \mu$m, $t_g = 0.35\ \mu$m, and $g = 10\ \mu$m.

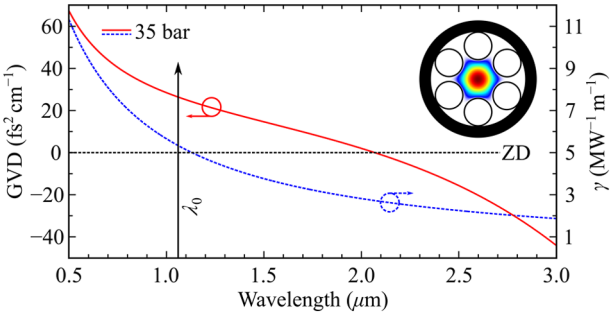

FIG. 2. The group-velocity dispersion (GVD, red solid line) and nonlinear parameter (γ, blue dashed line) in a negative-curvature fiber filled with xenon at 35 bar. The inset shows the intensity profile of the fundamental mode. ZD and λ_0 denote the zero dispersion and the pump wavelength, respectively.

γ when the fiber is filled with xenon at 35 bar pressure. There is a zero-dispersion wavelength (ZDW) at around 2.1 μm, with the normal-dispersion regime on the short-wavelength side and the anomalous-dispersion regime on the other side.

III. NONLINEAR PULSE PROPAGATION AND FREQUENCY CONVERSION

The propagation of femtosecond pulses in a nonlinear dispersive medium, such as a xenon-filled negative-curvature fiber, can be modeled using the generalized nonlinear Schrödinger equation [9,21]:

$$\frac{\partial A}{\partial z} = \sum_{n\geq 2} \frac{i^{n+1}}{n!}\beta_n \frac{\partial^n A}{\partial T^n} + i\gamma_0 \left(1 + \frac{i}{\omega_0}\frac{\partial}{\partial T}\right)|A|^2 A, \quad (1)$$

where $A\,(z, T)$ is the complex envelope of the optical field at propagation distance z; $T = t - \beta_1 z$ is time in the frame moving with the group velocity of the pulse $v_g = 1/\beta_1$; β_n is the nth-order Taylor-series expansion coefficient of the wave vector $\beta\,(\omega)$, evaluated at the carrier frequency ω_0; and γ_0 is the nonlinear parameter at the pump wavelength, which is determined by the filling gas species and its density. The time derivative in the nonlinear operator represents the effect of self-steepening characterized on a time scale $1/\omega_0$. For an atomic gas such as xenon, we can drop the Raman effect in the nonlinear term. Note that xenon may be subject to photoionization at high optical intensities. However, this has a negligible effect in our examples and Eq. (1) captures all the major effects of the femtosecond-pulse propagation studied below.

We consider the propagation of a 15-μJ pump pulse with a 30-fs duration in the near-infrared at 1.06-μm wavelength. Such a pulse can be obtained by compressing the output of a high-power fiber-laser system that is now made available commercially [22]. The pump wavelength in this example is deep in the normal-dispersion regime of the

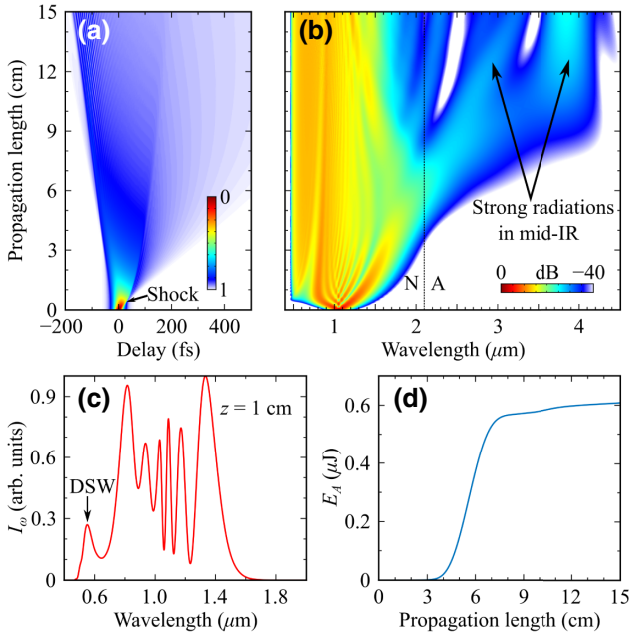

FIG. 3. The (a) temporal and (b) spectral evolutions of a 30-fs pump propagating in a xenon-filled negative-curvature fiber. The pump is centered at 1.06-μm wavelength and has an energy of 15 μJ. The vertical dotted line in (b) indicates the ZDW, where A and N denote the anomalous- and normal-dispersion regimes, respectively. (c) The normalized spectral intensity, I_ω, at $z = 1$ cm. The spectral band formed as a result of a dispersive shock wave (DSW) is marked with a vertical arrow. (d) The total energy in the anomalous-dispersion regime, E_A, as a function of the propagation length.

xenon-filled fiber, with its ZDW (2.1 μm) almost an octave away from the pump, as shown in Fig. 2. One major advantage of pumping in the normal-dispersion regime is that the output SC spectrum is relatively less sensitive to the fluctuations of the pump [16]. Figures 3(a) and 3(b) show the temporal and spectral evolutions of the pump propagating along a 15-cm length of the negative-curvature fiber. Note the exceptional spectral broadening, which covers a wide spectrum, 0.5–4.2 μm. In particular, strong radiations are observed in the mid-IR in the later stage of the propagation.

Soon after the launch of the pump, the combined effect of the self-phase modulation and the normal dispersion causes the low- (high-) frequency components generated in the central part of the pulse to advance (lag) toward the leading (trailing) edges of the pulse, respectively. This results in the pulse shape becoming rectangular, with steep edges on the sides. Then the self-steepening effect becomes significant, which further enhances the steep edge in its tail. As a result, the pulse becomes highly asymmetric in time, leaning toward its trailing edge. Further steepening leads to breaking of the trailing edge at $z \sim 0.40$ cm, with an oscillation forming at the back of the pulse. We can also describe the same phenomena in the frequency domain. The self-steepening introduces an asymmetric spectral broadening that enhances the short-wavelength side. In Fig. 3(b), we can see that the asymmetric extent of the spectrum significantly enhances the development of a separate sideband radiation known as a dispersive shock wave (DSW) [23] at 560 nm at $z \sim 0.55$ cm. This coincides with the appearance of the time-domain shock indicated by the arrow in Fig. 3(a). The pulse spectrum at $z = 1$ cm in Fig. 3(c) clearly shows the formation of a DSW at 560 nm. As we shall see, a phase-matched four-wave mixing (FWM) process is responsible for the DSW formation.

One important observation in Fig. 3(b) is that a substantial portion of the pump energy enters the anomalous-dispersion regime during the early spectral-broadening process. This, in fact, leads to further broadening of the spectrum, deeper into the mid-IR range, in the later stage of the propagation. Figure 3(d) shows that approximately 4.1% of the pump energy has entered the anomalous-dispersion regime after the pump having propagated 7 cm of the xenon-filled fiber. We stress that this happens despite having the ZDW far away—by almost an octave span—from the pump wavelength. Therefore, a simple explanation of the pump tunneling into the anomalous-dispersion region through self-phase modulation-induced broadening, as has been suggested in a number of previous reports where the pump was near the ZDW [24,25], cannot fully clarify the case presented here.

The phase mismatch $\Delta\beta$ plotted in Fig. 4(a) reveals how the conversion of the pump to two frequencies, one in the form of a DSW and the other deep into the anomalous-dispersion regime, occurs. The phase mismatch is calculated as follows [13]:

$$\Delta\beta = \beta(\omega) - \{\beta(\omega_0) + \beta_1(\omega_0)[\omega - \omega_0] + \gamma_0 P_0[\omega/\omega_0]\}, \quad (2)$$

where ω is the angular frequency, with ω_0 denoting that of the pump. P_0 is the peak power of the pump pulse and $\beta(\omega)$ is the wave vector. The strong effect of the self-steepening means that for an accurate determination of the phase-matching wavelengths, we need to account for the nonlinear-parameter dispersion by multiplying the γ_0 by ω/ω_0, as given in Eq. (2) [13]. Note that while Eq. (2) has been used widely for calculating the phase matching between a soliton and a dispersive wave (DW), recent studies have shown that the same equation can also be applied to obtain the radiation frequency when the system is pumped in the normal-dispersion regime [25,26].

In Fig. 4(a), the phase mismatch becomes zero at two wavelengths, one at 560 nm and the other at 2.55 μm, which also correspond to the wavelengths at which the radiation bands develop, as demonstrated in Fig. 4(b). Due to its proximity to the pump wavelength, as well as the

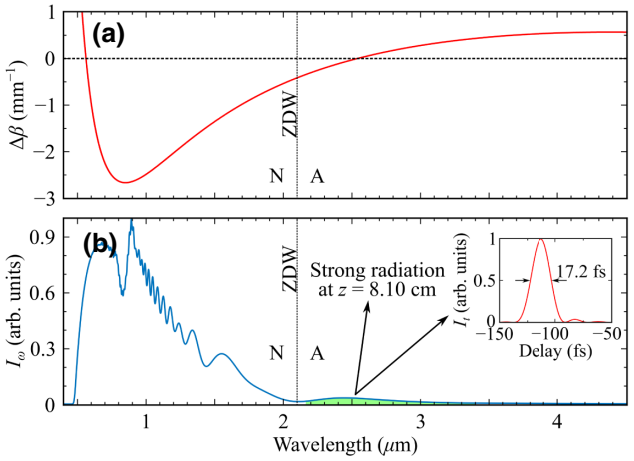

FIG. 4. (a) The phase mismatch ($\Delta\beta$) as a function of the wavelength. (b) The normalized spectral intensity, I_ω, at $z = 8.10$ cm. The inset shows the normalized time-domain intensity profile I_t of the green-shaded part of the spectrum.

blue-enhanced spectral broadening as a result of the self-steepening effect, the DSW band at 560 nm forms in the very early stage ($z < 1$ cm) of the pulse propagation. On the other hand, the 2.55-μm spectral band appears much later ($z > 7$ cm), due to the fact that this phase-matching wavelength is further out from the pump and hence it requires a longer propagation distance for the low-intensity tail in the pump to reach this point through self-phase modulation.

Once the seed photons reach the phase-matching wavelength at 2.55 μm, the conversion from the pump into the anomalous-dispersion regime becomes highly efficient. This is clearly noticeable in Fig. 3(d), where the energy in the anomalous-dispersion regime increases rapidly in the propagation length 5–8 cm. In fact, at $z = 8.10$ cm, the energy in the 2.55-μm spectral band, shown by the green shaded area in Fig. 4(b), is sufficient to form a higher-order optical soliton on its own. This spectral band translates into a pulse with a 17.2-fs full-width-at-half-maximum (FWHM) duration and a peak power of 25.55 MW in the time domain, as presented in the inset of Fig. 4(b). Taking into account the GVD and the nonlinear parameters of the xenon-filled fiber at 2.55-μm wavelength, this corresponds to a soliton with $N = 1.90$.

Further spectral broadening takes place in the later stage of propagation. In Fig. 3(b), the initial accumulation of the light at 2.55 μm leads to the formation of another spectral band at around 3.71 μm. This is also clearly evident in the spectrogram of the pulse at $z = 8.2$ cm presented in Fig. 5(a). We can see that the energy is moving toward longer wavelength and initiating the generation of another radiation in the mid-IR. In fact, this occurs while depleting the energy in the 2.55-μm spectral band. We find that this arises due to a degenerate FWM process. It satisfies the conservation of photon energy and momentum [21]:

$$2\omega_p = \omega_s + \omega_i, \tag{3}$$

$$2\beta_p = \beta_s + \beta_i + \Gamma_{\mathrm{NL}}, \tag{4}$$

where ω_p, ω_s, and ω_i are the angular frequencies of the pump, signal, and idler photons involved in the degenerate FWM process and β_p, β_s, and β_i are the wave vectors at the idler, pump, and signal, respectively. $\Gamma_{\mathrm{NL}} = 2\gamma_p P$ is the nonlinear correction term, where γ_p is the nonlinear coefficient at ω_p. A fixed-pulse peak power of $P = 25.55$ MW is used, which is shown in the inset of Fig. 4(b). In the degenerate FWM process, two pump photons are annihilated to create a signal-idler photon pair. Figure 5(b) is the phase-matching diagram as a function of the pump wavelength. It shows that for the 2.55-μm pump, the signal and idler photon pair are generated at 1.94 and 3.71 μm, respectively. In this study, the pump (2.55 μm) and the signal (1.94 μm) are presented at the early stage of the degenerate FWM process. Consequently, an idler is generated at 3.71 μm, as shown in Fig. 5(a). Note that the photons involved in this degenerate FWM process overlap at a delay of -0.1 ps. This means that the process will occur over an extended

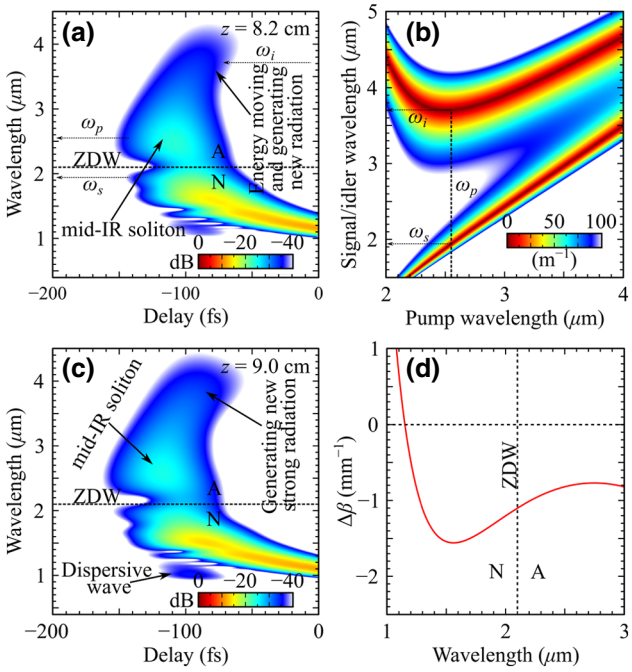

FIG. 5. (a) A spectrogram at $z = 8.2$ cm. (b) The phase-matching diagram of the degenerate FWM process as a function of the pump wavelength. The figure represents a signal-idler photon pair that satisfies the phase-matching conditions in Eqs. (3) and (4). The peak power of 25.55 MW is used in the calculations. ω_p, ω_s, and ω_i are the angular frequencies of the pump, the signal, and the idler photons involved in the degenerate FWM process. (c) A spectrogram at $z = 9.0$ cm. (d) The phase mismatch ($\Delta\beta$) as a function of the wavelength for the pump at 2.55 μm.

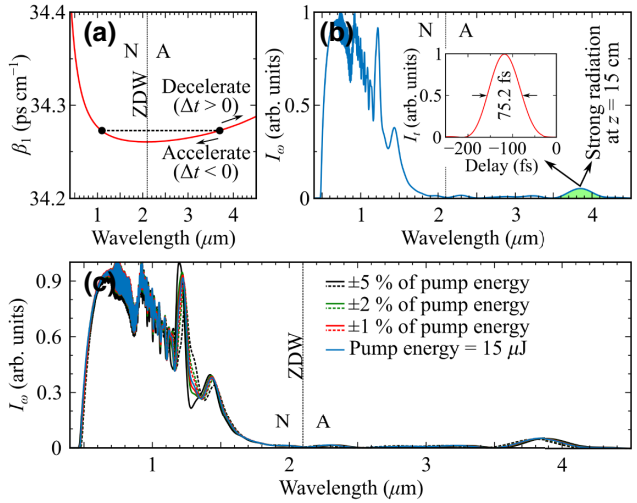

FIG. 6. (a) The group delay as a function of the wavelength. Δt is the initial time delay between the soliton and the DW. (b) I_ω at $z = 15$ cm. The inset shows the time-domain intensity profile I_t of the green-shaded part in the spectrum. (c) I_ω for different amounts of pump energy fluctuation. The solid and dotted lines indicate the percentage increment and decrement in the pump energy, respectively, except blue solid line.

length, thus enhancing the new spectral-band formation in the 3.71-μm spectral region.

In the presence of higher-order dispersion, the annihilating soliton centered at 2.55 μm involves another new radiation-generation process. At $z = 8.7$ cm, a DW is generated in the normal-dispersion regime at approximately 1.1 μm [27]. This is clearly evident in the spectrogram taken at $z = 9.0$ cm, presented in Fig. 5(c). We can see that the phase-matching condition given in Eq. (2) is met at the wavelength of the DW, as shown in Fig. 5(d). It should be mentioned that the energy in the DW is weak due to the small spectral overlap between the soliton and the DW and, therefore, it cannot be seen easily in Fig. 3(b). Moreover, since the soliton at 2.55 μm and its DW have different group velocities, they do not interact upon further propagation [28]. However, as we shall see, the DW contributes to another process that takes place in the later stage.

After its formation, the spectral band at 3.71 μm undergoes a further red shift, reaching 3.85 μm at $z = 15$ cm, as shown in Fig. 3(b). We note from the group delay $\beta_1 = 1/v_g$, plotted in Fig. 6(a), that the solitonlike radiation at 3.71 μm and the generated DW at 1.1 μm have similar group velocities. Moreover, when the 3.71-μm band forms at $z = 8.40$ cm, it marginally leads the DW, by approximately 60 fs, with a slightly smaller group velocity. Consequently, they undergo a collision, which induces the cross-phase modulation. In this case, the DW and the solitonlike radiation are temporally locked and during this time they copropagate along the fiber [29]. This results in the energy of the dispersive wave being converted to the mid-IR spectral band. The collision also causes both pulses to decelerate [29], red shifting the frequency of the mid-IR band while shifting the dispersive wave toward the blue, as shown in Fig. 6(a). Figure 6(b) indicates that a big chunk of the pump energy is in the 3.85-μm spectral band, at $z = 15$ cm. The green-shaded area translates to a $N = 1$ soliton with a 75.2-fs FWHM duration and a peak power of 4.96 MW in the time domain.

We also investigate the influence of the pump energy fluctuation on the output spectrum at $z = 15$ cm, as shown in Fig. 6(c). This study gives an indication of the experimental tolerance, i.e., the system's sensitivity to the pump noise. Note that the output-spectrum change is insignificant up to $\pm 5\%$ pump energy fluctuation, which clearly shows that the system is highly robust against the presence of noise in the pump.

IV. CONCLUSIONS

We find numerically a promising pathway to generate a supercontinuum in a nonlinear hollow-core fiber, using a high-power femtosecond pump source at 1.06-μm wavelength. We exploit the method of exciting a higher-order soliton in the mid-IR by pumping in the normal-dispersion regime, which further enhances the spectral broadening in the mid-IR region while preserving the output coherence. We show that a number of nonlinear optical effects, including the dispersive shock wave, phase-matched four-wave mixing, and soliton effects, are responsible for a wide spectral output of supercontinuum generation spanning over three octaves.

ACKNOWLEDGMENTS

We acknowledge the support of the Australian Research Council (ARC).

[1] S. Smirnov, J. D. Ania-Castanon, T. J. Ellingham, S. M. Kobtsev, S. Kukarin, and S. K. Turitsyn, Optical spectral broadening and supercontinuum generation in telecom applications, Opt. Fiber Technol. **12**, 122 (2006).
[2] S. Dupont, C. Petersen, J. Thøgersen, C. Agger, O. Bang, and S. R. Keiding, IR microscopy utilizing intense supercontinuum light source, Opt. Express **20**, 4887 (2012).
[3] J. T. Woodward, A. W. Smith, C. A. Jenkins, C. Lin, S. W. Brown, and K. R. Lykke, Supercontinuum sources for metrology, Metrologia **46**, S277 (2009).
[4] A. B. Seddon, A prospective for new mid-infrared medical endoscopy using chalcogenide glasses, Int. J. Appl. Glass Sci. **2**, 177 (2011).
[5] http://www.nktphotonics.com.
[6] J. Swiderski, High-power mid-infrared supercontinuum sources: Current status and future perspectives, Prog. Quantum Electron. **38**, 189 (2014).
[7] C. R. Petersen, U. Møller, I. Kubat, B. Zhou, S. Dupont, J. Ramsay, T. Benson, S. Sujecki, N. Abdel-Moneim, Z. Tang,

D. Furniss, A. Seddon, and O. Bang, Mid-infrared supercontinuum covering the 1.4–13.3 μm molecular fingerprint region using ultra-high NA chalcogenide step-index fibre, Nat. Photonics **8**, 830 (2014).

[8] G. Qin, X. Yan, C. Kito, M. Liao, C. Chaudhari, T. Suzuki, and Y. Ohishi, Ultrabroadband supercontinuum generation from ultraviolet to 6.28 μm in a fluoride fiber, Appl. Phys. Lett. **95**, 161103 (2009).

[9] J. C. Travers, W. Chang, J. Nold, N. Y. Joly, and P. S. J. Russell, Ultrafast nonlinear optics in gas-filled hollow-core photonic crystal fibers [Invited], J. Opt. Soc. Amer. B **28**, A11 (2011).

[10] A. Urich, R. R. J. Maier, F. Yu, J. C. Knight, D. P. Hand, and J. D. Shephard, Flexible delivery of Er:YAG radiation at 2.94 μm with negative curvature silica glass fibers: A new solution for minimally invasive surgical procedures, Biomed. Opt. Express **4**, 193 (2013).

[11] K. E. Lynch-Klarup, E. D. Mondloch, M. G. Raymer, D. Arrestier, F. Gérôme, and F. Benabid, Supercritical xenon-filled hollow-core photonic bandgap fiber, Opt. Express **21**, 13726 (2013).

[12] M. I. Hasan, N. Akhmediev, and W. Chang, Mid-infrared supercontinuum generation in supercritical xenon-filled hollow-core negative curvature fibers, Opt. Lett. **41**, 5122 (2016).

[13] F. Köttig, D. Novoa, F. Tani, M. C. Günendi, M. Cassataro, J. C. Travers, and P. St. J. Russell, Mid-infrared dispersive wave generation in gas-filled photonic crystal fibre by transient ionization-driven changes in dispersion, Nat. Commun. **8**, 813 (2017).

[14] M. Cassataro, D. Novoa, M. C. Günendi, N. N. Edavalath, M. H. Frosz, J. C. Travers, and P. St. J. Russell, Generation of broadband mid-IR and UV light in gas-filled single-ring hollow-core PCF, Opt. Express **25**, 7637 (2017).

[15] A. V. Husakou and J. Herrmann, Supercontinuum Generation of Higher-Order Solitons by Fission in Photonic Crystal Fibers, Phys. Rev. Lett. **87**, 203901 (2001).

[16] A. M. Heidt, Pulse preserving flat-top supercontinuum generation in all-normal dispersion photonic crystal fibers, J. Opt. Soc. Am. B **27**, 550 (2010).

[17] Y. Matsuura and K. Naito, Flexible hollow optical fiber bundle for infrared thermal imaging, Biomed. Opt. Express **2**, 65 (2011).

[18] H. H. P. T. Bekman, J. C. van den Heuvel, F. J. M. van Putten, and R. Schleijpen, Development of a mid-infrared laser for study of infrared countermeasures techniques, Proc. SPIE **5615**, 27 (2004).

[19] F. Yu and J. C. Knight, Negative curvature hollow-core optical fiber, IEEE J. Sel. Top. Quantum Electron. **22**, 4400610 (2016).

[20] M. I. Hasan, N. Akhmediev, and W. Chang, Empirical formulae for dispersion and effective mode area in hollow-core antiresonant fibers, IEEE J. Lightw. Technol. **36**, 4060 (2018).

[21] G. Agrawal, *Nonlinear Fiber Optics* (Academic Press, California, 2006), 4th ed.

[22] F. Köttig, F. Tani, C. M. Biersach, J. C. Travers, and P. St. J. Russell, Generation of microjoule pulses in the deep ultraviolet at megahertz repetition rates, Optica **4**, 1272 (2017).

[23] M. Conforti and S. Trillo, Dispersive wave emission from wave breaking, Opt. Lett. **38**, 3815 (2013).

[24] S. Roy, D. Ghosh, S. K. Bhadra, and G. P. Agrawal, Role of dispersion profile in controlling emission of dispersive waves by solitons in supercontinuum generation, Opt. Commun. **283**, 3081 (2010).

[25] K. E. Webb, Y. Q. Xu, M. Erkintalo, and S. G. Murdoch, Generalized dispersive wave emission in nonlinear fiber optics, Opt. Lett. **38**, 151 (2013).

[26] T. Roger, M. F. Saleh, S. Roy, F. Biancalana, C. Li, and D. Faccio, High-energy, shock-front-assisted resonant radiation in the normal dispersion regime, Phys. Rev. A **88**, 051801(R) (2013).

[27] N. Akhmediev and M. Karlsson, Cherenkov radiation emitted by solitons in optical fibers, Phys. Rev. A **51**, 2602 (1995).

[28] I. Cristiani, R. Tediosi, L. Tartara, and V. Degiorgio, Dispersive wave generation by solitons in microstructured optical fibers, Opt. Express **12**, 124 (2004).

[29] J. Gu, H. Guo, S. Wang, and X. Zeng, Probe-controlled soliton frequency shift in the regime of optical event horizon, Opt. Express **23**, 22285 (2015).